

Characterizing the High-Velocity Stars of RAVE: The Discovery of a Metal-Rich Halo Star Born in the Galactic Disk

K. Hawkins^{1*}, G. Kordopatis^{1,2}, G. Gilmore¹, T. Masseron¹, R. F. G. Wyse³, G. Ruchti⁴, O. Bienaymé⁵, J. Bland-Hawthorn⁶, C. Boeche⁷, K. Freeman⁸, B. K. Gibson⁹, E. K. Grebel⁷, A. Helmi¹⁰, A. Kunder², U. Munari¹¹, J. F. Navarro¹², Q. A. Parker^{13,14}, W. A. Reid¹³, R. D. Scholz², G. Seabroke¹⁵, A. Siebert⁵, M. Steinmetz², F. Watson¹⁴, T. Zwitter¹⁶

¹*Institute of Astronomy, Madingley Road, Cambridge CB3 0HA, UK*

²*Leibniz-Institut für Astrophysik Potsdam (AIP) An der Sternwarte 16, D-14482 Potsdam, Germany*

³*Physics and Astronomy Department, Johns Hopkins University, 3400 North Charles Street, Baltimore, MD 21218, USA*

⁴*Lund Observatory, Department of Astronomy and Theoretical Physics, Box 43, SE-22100 Lund, Sweden*

⁵*Observatoire astronomique de Strasbourg, Université de Strasbourg, CNRS, UMR 7550, 11 rue de l'Université, F-67000 Strasbourg, France*

⁶*Sydney Institute for Astronomy, School of Physics A28, NSW 2006, Australia*

⁷*Astronomisches Rechen-Institut, Zentrum für Astronomie der Universität Heidelberg, Mönchhofstr. 12-14, 69120 Heidelberg, Germany*

⁸*Research School of Astronomy and Astrophysics, Australian National University, Cotter Rd., ACT 2611 Weston, Australia*

⁹*Jeremiah Horrocks Institute, University of Central Lancashire, Preston, PR1 2HE, U.K.*

¹⁰*Kapteyn Astronomical Institute, University of Groningen, PO Box 800, NL-9700 AV Groningen, the Netherlands*

¹¹*INAF Astronomical Observatory of Padova, 36012 Asiago (VI), Italy*

¹²*CIAR Senior Fellow, University of Victoria, Victoria, BC, Canada V8P 5C2*

¹³*Research Centre for Astronomy, Astrophysics and Astrophotonics, Macquarie University, Sydney, NSW 2109, Australia*

¹⁴*Australian Astronomical Observatory, 105 Delhi Road, North Ryde, PO Box 915, North Ryde, NSW 1670, Australia*

¹⁵*Mullard Space Science Laboratory, University College London, Holmbury St Mary, Dorking, RH5 6NT, UK*

¹⁶*Faculty of Mathematics and Physics, University of Ljubljana, Jadranska 19, SI-1000 Ljubljana, Slovenia*

Accepted 2014 December 02. Received 2014 December 01; in original form 2014 November 05

ABSTRACT

We aim to characterize high-velocity (HiVel) stars in the solar vicinity both chemically and kinematically using the fourth data release of the RAdial Velocity Experiment (RAVE). We used a sample of 57 HiVel stars with Galactic rest-frame velocities larger than 275 km s^{-1} . With 6D position and velocity information, we integrated the orbits of the HiVel stars and found that, on average, they reach out to 13 kpc from the Galactic plane and have relatively eccentric orbits consistent with the Galactic halo. Using the stellar parameters and $[\alpha/\text{Fe}]$ estimates from RAVE, we found the metallicity distribution of the HiVel stars peak at $[\text{M}/\text{H}] = -1.2$ dex and is chemically consistent with the inner halo. There are a few notable exceptions that include a hypervelocity star (HVS) candidate, an extremely high-velocity bound halo star, and one star that is kinematically consistent with the halo but chemically consistent with the disk. High-resolution spectra were obtained for the metal-rich HiVel star candidate and the second highest velocity star in the sample. Using these high-resolution data, we report the discovery of a metal-rich halo star that has likely been dynamically ejected into the halo from the Galactic thick disk. This discovery could aid in explaining the assembly of the most metal-rich component of the Galactic halo.

Key words: Galaxy: halo–Galaxy: abundances–Galaxy: kinematics and dynamics

1 INTRODUCTION

The advent of large spectroscopic surveys in the last decade has opened a new field of investigation: high-velocity (HiVel) stars. These stars are rare objects, defined by having velocities well above

the typical speed of the stars one might expect (e.g. $>80 \text{ km s}^{-1}$ relative to the Sun, Schuster & Nissen 1988), but below the Galactic escape speed. HiVel stars are intriguing in part because they can provide insight to the mechanism that produce their velocities. The origin of these HiVel stars can also provide useful information about the environments from which they are produced. While recent studies have used only the kinematics of high-velocity stars

* E-mail: khawkins@ast.cam.ac.uk

to obtain an estimate of the Galaxy’s mass (e.g. [Smith et al. 2007](#); [Piffl et al. 2014](#)), there have been only a few studies aimed at combining their chemical and kinematic information to get a picture of where these stars are produced and what caused them to achieve such high-velocities. Therefore, we aim to fill this gap by combining both the kinematics and chemistry of these HiVel stars using the RAdial Velocity Experiment ([Steinmetz et al. 2006](#), RAVE) to discern if they are consistent with any particular component of the Milky Way and what may have produced them.

[Ryan & Smith \(2003\)](#) studied a sample of 10 intermediate-metallicity HiVel stars and found that most of them resemble the thick disk yet the HiVel stars of other studies (e.g. [Schuster et al. 2006](#)) suggested that HiVel stars are metal poor. This raises the question what is the chemical distribution (in $[\text{Fe}/\text{H}]$ and $[\alpha/\text{Fe}]^1$ spaces) of HiVel stars in the solar neighbourhood? The answers to this question will ultimately aid in constraining where HiVel stars are born and thus help constrain models for how they are produced. In turn, this will help develop a better understanding for the assembly of the Galactic halo for which many of these HiVel stars are thought to currently reside. For example, if the metallicity distribution of HiVel stars is significantly more metal-rich compared to the halo, and if the $[\alpha/\text{Fe}]$ distribution is comparable to the disk, it may support the suggestion of [Bromley et al. \(2009\)](#) that the metal-rich tail of the Galactic halo may have come from kinematically heated, stars which formed in the disk.

These ‘runaway’ disk stars described above are a subclass of HiVel stars and were first identified by [Humason & Zwicky \(1947\)](#). Runaway disk stars can provide an invaluable connection between star formation in the Galactic disk and halo. These stars are rare and described by peculiar velocities up to 200 km s^{-1} and are thought to have formed in the disk and ejected into the halo. Theoretically, runaway stars can be produced through a number of different mechanisms including: (1) binary supernova ejection (e.g. [Blaauw 1961](#); [Portegies Zwart 2000](#)) and (2) dynamical ejection due to 3- and 4-body encounters (e.g. [Poveda, Ruiz & Allen 1967](#); [Bromley et al. 2009](#)). It is thought that these above mechanisms can produce both low-mass and high-mass runaway stars. Yet most of the literature regarding runaway stars focuses on high-mass O and B type stars. This is likely because observationally O and B type runaway stars are bluer compared to normal, low-mass halo stars among where they were found (e.g. [Poveda, Allen & Hernández-Alcántara 2005](#)). Characterizing HiVel stars, particularly in a data set with evolved low-mass stars, will allow us to search for these elusive stars.

Another intriguing subclass of HiVel stars is hypervelocity stars (HVSs), which are racing through space at above the escape speed of the Milky Way. These stars are thought to be produced via three-body interactions between a binary star system and the super massive black hole at the Galactic Centre ([Hills 1988](#)). However, other production mechanisms have been proposed to explain stars which do not seem to originate in the Galactic Centre (e.g. [Yu & Tremaine 2003](#); [Przybilla et al. 2008](#); [Heber et al. 2008](#); [Tillich et al. 2009](#)). HVSs and HiVel stars can be used to infer many aspects about the Milky Way such as Galactic escape speed, and Galactic mass ([Smith et al. 2007](#); [Piffl et al. 2014](#)), and HVS, in particular, offer a window into the mass function and dynamics of the environment near the massive black hole at the Galactic center ([Portegies Zwart et al. 2006](#); [Löckmann, Baumgardt &](#)

[Kroupa 2008](#); [Löckmann & Baumgardt 2008](#); [Lu, Yu & Lin 2007](#); [Brown, Geller & Kenyon 2012](#)). The benefit of finding and characterizing these HiVel stars and HVS can be translated into better understanding the structure, dynamics and evolution of the Milky Way. Most of the confirmed HVSs are early-type O and B type stars due to the selection bias of current HVS surveys. In recent years, there have been a few HVS candidates that are more evolved, later-type stars ([Brown, Geller & Kenyon 2012, 2014](#); [Palladino et al. 2014](#)). RAVE mostly targets late-type dwarfs and giants, and thus any HVS candidates will add to a now growing list of late-type HVSs candidates. Many studies have been devoted solely to search for HVS through dedicated surveys (e.g. [Brown, Geller & Kenyon 2012, 2014](#)) as well as large surveys such as the Sloan Digital Sky Survey ([Kollmeier et al. 2010](#); [Palladino et al. 2014](#); [Zhong et al. 2014](#), SDSS). However, HVS have not been searched for in the RAVE data set. In this paper, we can naturally explore this by searching for HiVel stars.

While the main purpose of our study is to characterize, kinematically and chemically, HiVel stars, we will also investigate the runaway and hypervelocity candidates, for which we also have high-resolution spectra. In this paper, we start by searching for these rare HiVel stars using the RAVE data set and a series of selection criteria (described in section 2). We then move on to discuss the kinematic, chemical distribution of our HiVel sample in section 3. Using these distributions, we search for and suggest the origins of HVS and runaway star candidates. We summarize our key findings, put our findings into context with other studies and conclude in section 4.

2 A SAMPLE OF HIGH-VELOCITY STARS

2.1 RAVE Survey Data Release 4

One of the easiest ways to search for HiVels is to use large astronomical surveys with high quality kinematic measurements, such as radial velocity (RV) and proper motions, etc. To this end, we make use of the fourth data release of RAVE ([Kordopatis et al. 2013a](#), RAVE DR4). RAVE has obtained data using the multi-object spectrograph on the 1.2-m Australian Astronomical Observatory’s UK Schmidt Telescope in Australia. The RAVE DR4 catalogue has reduced spectra and radial velocities (RVs) for nearly a half-million stars and represents one of the largest available catalogues to date. RAVE spectra are moderate resolution ($R = \lambda/\Delta\lambda \sim 7000$) around the Ca II triplet covering the wavelength range of $8410 - 8795 \text{ \AA}$. For more information regarding RAVE, we refer the reader to the data release papers: [Steinmetz et al. \(2006\)](#); [Zwitter et al. \(2008\)](#); [Siebert et al. \(2011\)](#); [Kordopatis et al. \(2013a\)](#) and the review of [Kordopatis \(2014\)](#). In addition to the accurate RV estimates, with errors on the order of 2 km s^{-1} , DR4 contains stellar parameters and distances with errors of about 10-20 percent. RAVE also has an associated chemical abundance catalogue, which provides estimates of 6 elements including Fe and several α -elements (described in [Boeche et al. 2011](#)). The chemical pipeline used a hybrid approach of inferring abundance using the curves-of-growth for different elements as well as a penalizing χ^2 technique of synthetic grid matching. [Boeche et al. \(2011\)](#) was able to determine the abundances of $[\alpha/\text{Fe}]$ and iron with a mean error of $\sim \pm 0.2$ dex. This work will refer to $[\text{M}/\text{H}]$ as metallicity and the traditional $[\text{Fe}/\text{H}]$ as the iron abundance. $[\text{M}/\text{H}] \sim [\text{Fe}/\text{H}]$ under the assumption that the star follows the standard α -enrichment scheme observationally seen in the Milky Way:

¹ The α -elements include those which have atomic numbers as a multiple of 4, such as Mg, Ti, Si, and Ca. $[\alpha/\text{Fe}]$ in this paper is defined as the mean abundance of these α -elements.

- (i) $[\alpha/Fe] = 0.0$ dex for $[Fe/H] \geq 0$ dex
- (ii) $[\alpha/Fe] = -0.4 \times [Fe/H]$ dex for $-1 \leq [Fe/H] < 0$ dex
- (iii) $[\alpha/Fe] = 0.4$ dex for $[Fe/H] < -1.0$ dex

If these criteria do not hold, the RAVE metallicity does not equal $[Fe/H]$. The trend for RAVE stars is such that $[M/H] > [Fe/H]$ for low metallicity (Kordopatis et al. 2013a, Figure 28).

2.2 High-Resolution Data

A few targets, namely several interesting HiVel and HVS candidates were followed up in high-resolution to enable detailed elemental abundance analysis. The high-resolution ($R \sim 31500$) spectra were obtained using the ARC Echelle Spectrograph (ARCES) on the Apache Point Observatory (APO) 3.5-m telescope. The spectra were reduced in the standard way: bias subtraction, extraction, flat field division and stacking using the echelle package of IRAF². The final high-resolution spectra have a typical SNR ~ 90 -200 pixel⁻¹ in the wavelength region of 4500 – 9000 Å.

Stellar parameters (T_{eff} , $\log g$, microturbulent velocity, ξ , and $[Fe/H]$) have been derived spectroscopically using the Brussels Automatic Code for Characterizing High accuracy Spectra (BACCHUS, Masseron et al., in preparation) code. The current version uses a grid of MARCS model atmospheres (Gustafsson et al. 2008), a specific procedure for interpolating the model atmosphere thermodynamical structure within the grid (Masseron 2006) and the radiative transfer code TURBOSPECTRUM (Alvarez & Plez 1998; Plez 2012). Atomic lines are sourced from VALD, Kupka & Ryabchikova (1999), Hill et al. (2002), and Masseron (2006). Linelists for the molecular species are provided for CH (T. Masseron et al. 2014, in press), and CN, NH, OH, MgH and C2 (T. Masseron, in prep); the lines of SiH molecules are adopted from the Kurucz linelists and those from TiO, ZrO, FeH, CaH from B. Plez (private communication).

The stellar parameters determination relies on a list of selected Fe lines. The first step consists in determining accurate abundances for the selected lines using the abundance module for a given set of T_{eff} and $\log g$. The abundance determination module proceeds in the following way: (i) a spectrum synthesis, using the full set of (atomic and molecular) lines, is used for local continuum level finding; (ii) cosmic and telluric rejections are performed; (iii) local signal-to-noise is estimated; (iv) a series of flux points contributing to a given absorption line is selected. Abundances are then derived by comparing the observed spectrum with a set of convolved synthetic spectra characterized by different abundances. Four different diagnostics are used: χ^2 fitting, core line intensity comparison, global goodness-of-fit estimate, and equivalent width comparison. A decision tree then rejects the line, or accepts it keeping the best matching abundance.

The second step consists in deducing the equivalent widths of Fe lines using the stellar parameter module. The last step of the procedure consists in injecting the derived equivalent widths in TURBOSPECTRUM to derive abundances for a grid of 27 neighboring model atmospheres (including three T_{eff} , three $\log g$ and three microturbulence velocities, covering the parameter space of interest). For each model, the slopes of abundances against excitation potential and against equivalent widths, as well as Fe I and Fe II lines abundances are computed. The final parameters are determined by

forcing that the ionization equilibrium is fulfilled, and that simultaneously null slopes for abundances against excitation potential and against equivalent widths are encountered. The whole procedure is iterated twice per star, a first guess using the RAVE stellar parameters as a starting point and then again with a different starting point. This was done to obtain an independent set of stellar parameters compared to RAVE. We adopted the parameters from the second iteration for each star, however both iterations produce parameters that are in very good agreement. Individual elemental abundances in each of the absorption features were determined using a χ^2 minimization technique to synthesized spectra. We visually inspected all fits in order to ensure the abundances were determined accurately. We take the mean and dispersion of the individual line abundances as the abundance and internal error respectively.

2.3 Distances and Proper Motions

Proper motions were sourced from the fourth US Naval Observatory CCD Astrograph Catalogue (UCAC4), which contains proper motions for over 100 million objects. We choose UCAC4 because the error in proper motion is generally smaller compared to other catalogues (see Binney et al. 2014b, for discussion). UCAC4 reaches a limiting magnitude of $R = 16$, with a peak in the formal uncertainty on the order of 4 mas/year (Zacharias et al. 2013). The small uncertainties in proper motion make them ideal for estimating the total velocity vector accurately. Following the suggestion of Zacharias et al. (2013), we discard any star with an uncertainty in proper motion larger than 10 mas/year to avoid stars which have been labeled as ‘problematic’ by the UCAC4. For most stars the UCAC4 proper motions are, within the errors of proper motion, in good agreement with other proper motion catalogues. Stars with no proper motions were discarded because the full kinematics cannot be explored without estimated proper motions. All stars that had a double star flag not equal to zero (it was either identified as a component of a double star system or it could not be ruled out as a double star) were excluded. Distances were determined from the estimated spectrophotometric parallax for each star using a method described by Binney et al. (2014a). We selected only stars that have estimated parallaxes because we need the distance to study the full kinematics of the stars. We expect typical uncertainties in parallax for our sample are on the order of 25 per cent (see Binney et al. 2014a, for more details).

2.4 Selection of High-Velocity Stars

To obtain robust data, we employed the quality control cuts laid out by Kordopatis et al. (2013a) as well as some additional cuts described here.

(i) The signal-to-noise ratio (SNR) must be larger than 20 pixel⁻¹. This cut was chosen to ensure that we are selecting out spectra that have well known uncertainties in the stellar parameters, and chemical abundances. Where there is more than one entry in the database we accept the entry with the highest SNR.

(ii) The errors in the heliocentric RV (HRV) must be lower than 10 km s⁻¹. This is to obtain precise RV measurements in order to constrain the full space motion. This cut is also necessary for accurate parameter estimation (Kordopatis et al. 2013a).

(iii) The estimated $\log g$ must be larger than 0.5 dex. Stars with $\log g$ less than 0.5 dex are much more likely to be treated in a problematic way during the stellar parameter estimation (Kordopatis et al. 2013a).

² Distributed by NOAO, operated by AURA under cooperative agreement with the NSF.

(iv) Calibrated metallicity $[M/H]$ must be larger than -5 dex (measured by the stellar parameter pipeline). Stars below this were discarded stars because the stellar parameter estimation (Kordopatis et al. 2013a) pipeline was not designed to perform for these stars.

(v) Calibrated T_{eff} must be between 4000 K and 7000 K. This was based on the range bounded by the synthetic library with which the RAVE chemical pipeline used.

(vi) The estimated stellar rotation velocity of the star, $V_{\text{rot}} < 50 \text{ km s}^{-1}$. This cut allowed us to discard stars that the stellar parameter and chemical pipelines would be likely to not produce reliable results.

(vii) All spectroscopic morphological flags defined by Matijević et al. (2012) must be ‘normal’. This criterion minimized the chance of binary star contamination or highly uncertain stellar parameters and distances (Kordopatis et al. 2013a; Binney et al. 2014a; Boeche et al. 2011).

(viii) The DR4 algorithm convergence parameter (algo_conv) must not equal 1. We used this cut to ensure the stellar parameter pipeline converged (Kordopatis et al. 2013a)

(ix) The value frac (i.e. the fraction of the spectrum that matches the model in a satisfactory way) associated with the chemical pipeline must be greater than 0.7.

(x) The χ^2 associated to the chemical pipeline must be lower than 2000. This cut along with the value frac cut was used to confirm that the spectra were adequately fit with no glaring errors in the continuum (Boeche et al. 2011).

(xi) The Tonry-Davis correlation coefficient, which is a measure of the quality of the template fit for each stellar spectra during the RV measurement, must be larger than 10 (Piffl et al. 2014; Steinmetz et al. 2006; Kordopatis et al. 2013a).

A total of 274 481 objects passed the 11 quality cuts described above. We corrected the HRVs for solar and local standard of rest (LSR) motion to obtain a RV relative to the Galactic rest-frame (GRV) using the following formula:

$$\text{GRV} = \text{HRV} + (U_{\odot} \cos l + (V_{\odot} + V_{\text{LSR}}) \sin l) \cos b + W_{\odot} \sin b, \quad (1)$$

where $U_{\odot}, V_{\odot}, W_{\odot}, V_{\text{LSR}}, l, b$ are the 3-dimensional solar velocity, the velocity of the local standard of rest (assumed to be 220 km s^{-1}), the Galactic longitude and latitude, respectively. For reference, the velocity convention adopted by this work is: U is positive if directed toward the Galactic Centre ($l = 0^{\circ}, b = 0^{\circ}$), V is positive along the direction of rotation ($l = 90^{\circ}, b = 0^{\circ}$) and W is positive if pointed toward the North Galactic Pole ($b = 90^{\circ}$). In this convention, the Sun’s orbital velocity vector $\vec{v}_{\odot} = [U_{\odot}, V_{\odot}, W_{\odot}] = [14.0, 12.24, 7.25] \text{ km s}^{-1}$, $V_{\text{LSR}} = 220 \text{ km s}^{-1}$ and position = $[8.28, 0, 0] \text{ kpc}$ (Schönrich 2012).

We initially selected objects with an absolute $|\text{GRV}| > 300 \text{ km s}^{-1}$ in regions where most of the disk velocity is along the line-of-sight (at $l = 90 \pm 50^{\circ}$ and $270 \pm 50^{\circ}$) and $|\text{GRV}| > 275 \text{ km s}^{-1}$ elsewhere. This requirement was designed to cut out most of the disk contamination that would otherwise occur owing to the geometry. These boundaries are selected to be just above the speed one would expect when considering disk rotation and velocity dispersion. Lowering the cut on GRV would cause larger contamination from ordinary disk stars while increasing the threshold decreases the total sample size. The selection of our sample can be found in Figure 1. The open circle, star and triangle refers to three interesting targets including J154401.1-162451, J221759.1-051149, and J161055.6-112009 (henceforth J1544, J2217, and J1610) respectively, that we discuss in the further detail in later sections. The sig-

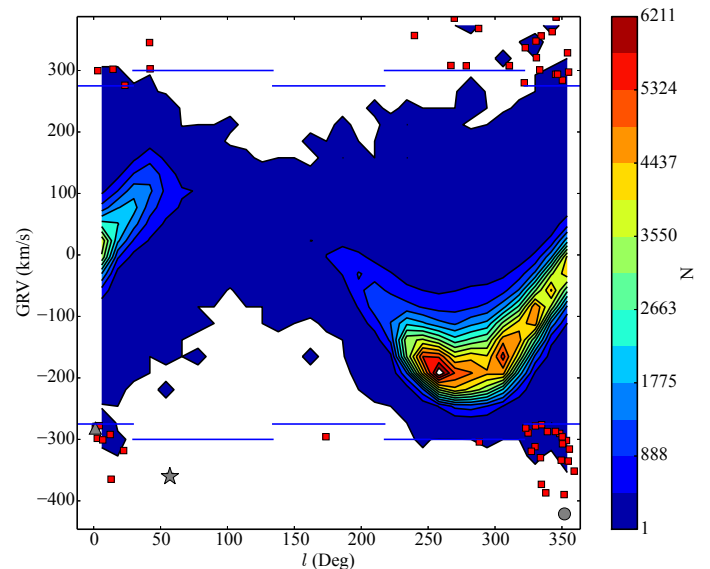


Figure 1. The selected HiVel targets (red squares) in l -Galactic relative radial velocity (GRV) space. The blue lines indicate the selection criteria where the $|\text{GRV}| > 300 \text{ km s}^{-1}$ near galactic latitudes pointed in the direction of disk rotation ($l = 90 \pm 50^{\circ}$ and $270 \pm 50^{\circ}$) and $|\text{GRV}| > 275 \text{ km s}^{-1}$ elsewhere. The contours show the full RAVE DR4 sample from which the HiVel targets were selected. The color in all 2D density diagrams, like this one, represents the number of stars in each density contour for the full RAVE dataset. The gray circle, star and triangle refers to three interesting targets, namely J1544, J2217, and J1610 respectively, that we discuss in the further detail in later sections.

nal of the disk can be seen as the sinusoidal-like high-density path seen in Figure 1. This is a geometric effect caused by the fact that disk stars move along rotation and thus when we observe at angles directed towards or away from rotation, most of the disk star velocity will be in the line-of-sight direction. The high density around $l = 270^{\circ}$ with $\text{GRV} \sim -220 \text{ km s}^{-1}$ represents the disk because at that Galactic longitude, the total velocity vector is primarily in the line-of-sight direction.

We further required the distances, proper motions (with uncertainties less than 5 mas/yr) and metallicities to be known. There are 57 stars in our final sample that passed all of the 11 quality control cuts and the kinematic cut described above. Piffl et al. (2014) used a sample of 76 HiVel stars in RAVE to determine the mass of the Milky Way halo. Our sample has fewer HiVel stars than Piffl et al. (2014) which is a result of the fact that they use a much lower GRV cut (200 km s^{-1}) than we do by selecting for a counter-rotating population assumed to be the halo population. Our kinematic selection criteria in l -GRV space can be seen in Figure 1. It is important to note that we choose to select our HiVel stars on the GRV rather than the full space motion because of the smaller error in GRV, on the order of a few km s^{-1} , compared to the error on the full space motion (few tens of km s^{-1}). Most of the HiVel stars in our sample are giant stars (Figure 2) and located within 5 kpc of the Sun (Figure 3). RAVE is run out of the Southern Hemisphere and as a result the spatial distribution of the selected HiVel stars is not symmetric around the Sun.

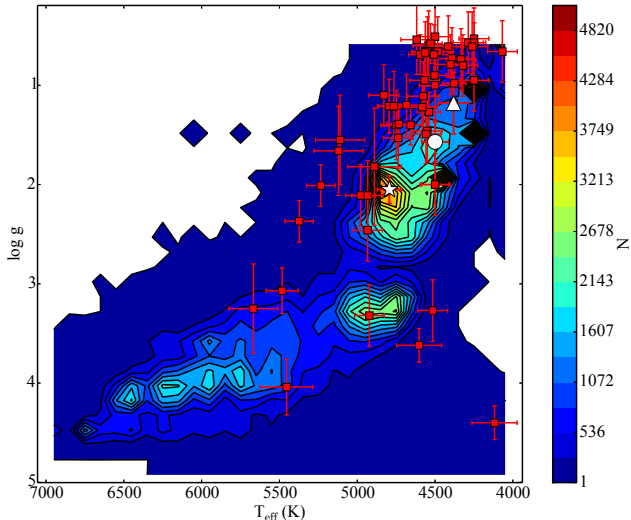


Figure 2. Contours of the $T_{\text{eff}} - \log g$ for stars in the RAVE sample with the HiVel stars (red squares) shown as being primarily giant stars. The open circle, star and triangle are the same as in Figure 1.

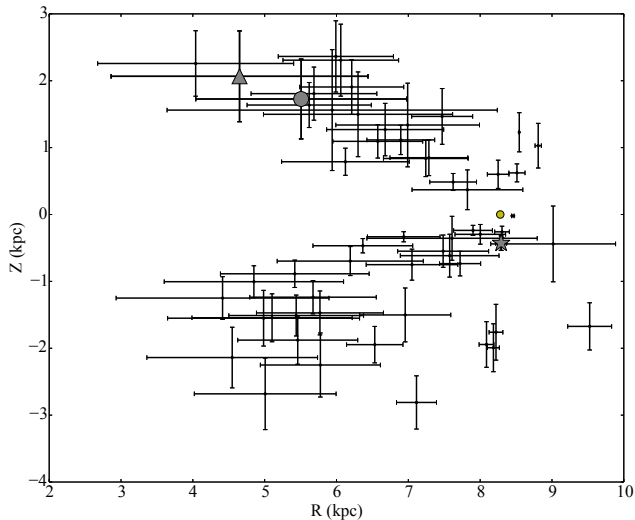


Figure 3. The position of our HiVel stars relative to the Galaxy. For reference the Sun (yellow circle) is at $(R, Z) = (8.28, 0)$ kpc. The gray circle, star and triangle are the same as in Figure 1.

2.5 Full Space Velocity and Stellar Orbits

We fully resolve the space velocity and position vectors in order to study the orbital parameters of our sample. The right ascension (α), declination (δ), and distances for each source yield a full 3D position vector relative to the Galaxy. These vectors are related by the Sun’s Galactocentric position ($\vec{r}_{\odot} = [8.28, 0, 0]$ kpc) such that $\vec{r} = \vec{r}_* + \vec{r}_{\odot}$ (Schönrich 2012). Furthermore, the proper motions give two dimensions of velocity within the plane of the sky, $\vec{\mu}$. We use the estimated proper motion, distance, and RV to construct a current velocity vector (relative to the Galactic-rest frame) via Johnson & Soderblom (1987). Uncertainties in the current position and velocity vector were determined using a Monte Carlo approach with a thousand realizations, randomly varying the uncertainties of all of the observables and recalculating the position and velocity

vectors and studying the final distribution, similar to the approach used by Gratton et al. (2003) and Boeche et al. (2013). We excluded two stars with uncertainties in the total space velocity larger than 200 km s^{-1} as it would be difficult to constrain their total space motions.

To obtain the orbital parameters for our HiVel sample, we integrated the orbit of a test particle through an assumed Galactic potential (Φ) which is a sum of the potential of a logarithmic halo ($\Phi_{\text{halo}}(r)$), Miyamoto-Nagai disk ($\Phi_{\text{disk}}(R, z)$), and a Hernquist bulge ($\Phi_{\text{bulge}}(r)$). We made use of the same parameter choices as Johnston, Spergel & Hernquist (1995).

$$\Phi_{\text{halo}}(r) = \frac{v_0^2}{2} \ln(r^2 + d^2), \quad (2)$$

where v_0 is a characteristic velocity of 186 km s^{-1} with a scale length, d , of 12.0 kpc.

$$\Phi_{\text{disk}}(R, z) = -\frac{GM_{\text{disk}}}{\sqrt{R^2 + (a + \sqrt{z^2 + b^2})^2}}, \quad (3)$$

where the M_{disk} is the mass of the disk assumed to be $10^{11} M_{\odot}$, a and b are scale lengths set to 6.5 kpc, and 0.26 kpc, respectively.

$$\Phi_{\text{bulge}}(r) = -\frac{GM_{\text{bulge}}}{r + c}, \quad (4)$$

where M_{bulge} is the mass of the bulge and is set to $3.4 \times 10^{10} M_{\odot}$ and c is a scale-length set to 0.7 kpc. In the above definitions $r = \sqrt{x^2 + y^2 + z^2}$ and $R = \sqrt{x^2 + y^2}$. Using this potential, we confirmed the circular speed, v_{circ} , at the solar radius of 8.28 kpc to be $v_{\text{circ}} = 224 \text{ km s}^{-1}$ and an orbital period for the local standard of rest (LSR) at this radius of 220 Myr consistent with Schönrich (2012). We also verified that energy and angular momentum is conserved in all orbital integrations to at least one part in a million or better.

To better understand the kinematics of our stars, we estimated the maximum distance above the Galactic plane (denoted Z_{max}) and the eccentricity from the orbital integration. We define the eccentricity as a function of the apogalactic distance, r_{ap} , and the perigalactic distance, r_{per} , such that $e = (r_{\text{ap}} - r_{\text{per}}) / (r_{\text{ap}} + r_{\text{per}})$. Uncertainties in the orbital integrations were estimated in a similar Monte Carlo approach as above (the initial conditions were varied to within their uncertainties) with 100 orbital integrations. We find the uncertainty in the eccentricity is less than 0.15.

3 RESULTS: METAL-POOR HIGH-VELOCITY STARS, EJECTED DISK STARS AND HYPERVELOCITY STARS

In this section we discuss the kinematic (section 3.1) and chemical (section 3.2) distributions of our HiVel star sample. By combining the results of these two sections we discuss the discovery of a metal-rich halo star that likely originated in the Galactic disk and put forward a HVS candidate.

3.1 Kinematics of High-Velocity Stars

We first studied the kinematics of our HiVel sample using a Toomre diagram (Figure 4), which quantifies different Galactic components using the velocity vector. It is important to note that the velocities in the Toomre diagram are relative to the LSR and thus the HVS boundary (green line, Figure 4), which must be converted to a non-rotating reference frame, was shifted by $V = -220 \text{ km s}^{-1}$.

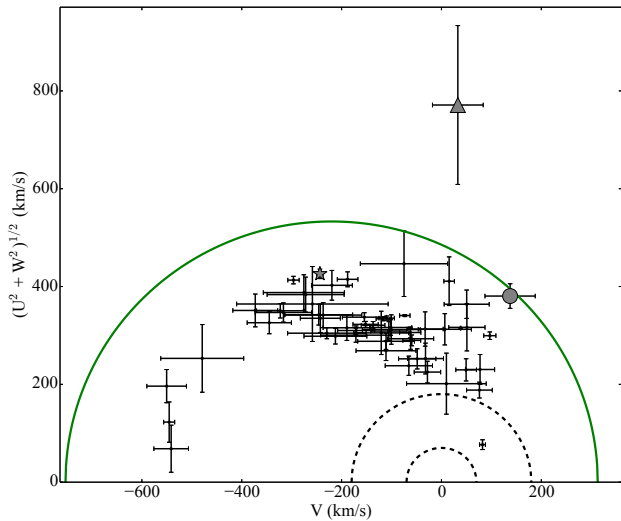


Figure 4. Toomre diagram for the HiVel sample. All velocities are relative to the LSR. The 2 black dashed rings show roughly the boundaries of the thin disk and thick disk at a constant velocity of 70 km s^{-1} , 180 km s^{-1} respectively (Venn et al. 2004). We can see that most of our HiVel stars belong to the halo kinematically. The green solid line represents a constant galactic-rest frame velocity of 533 km s^{-1} , and is thus shifted relative to the other velocities. A star above this boundary may be HVS candidate pending its position. We find one HVS candidate with a total Galactic rest frame velocity larger than 800 km s^{-1} (more than $1\text{-}\sigma$ above the escape speed). There are two stars, namely J1610 and J154401.1-16245, which have velocities above HVS limit. The gray circle, star and triangle are the same as in Figure 1.

From inspection, there are two stars which sit at or above the HVS boundary (green line, Figure 4). We note that the HVS boundary is position dependent. For simplicity, we choose the escape speed at the solar circle as an illustrative HVS boundary on the Toomre diagram. However, a true HVS candidate must have a velocity higher than the escape speed at its position. There is also one star that has disk-like kinematics and is likely with the high-velocity tail of the thin disk or disk-like contaminants. Using the rough boundaries that kinematically separate the thin-disk, thick disk and halo of Venn et al. (2004) for example, we found that most of our HiVel stars exist in the halo-region of the Toomre diagram which means these stars are likely be on highly elliptical orbits reaching out to a maximum distances from the Galactic plane, Z_{max} , larger than 10 kpc with eccentricities of $e \gtrsim 0.5$. Adopting larger boundaries in the Toomre diagram that kinematically separate the thin-disk, thick disk and halo would result in a slight contamination by the thick disk.

We further studied the kinematics of our sample by comparing the e and Z_{max} (Figure 5). The power of the e - Z_{max} plane is the ability to sort out stars of similar orbits, because e describes the shape of the orbit and Z_{max} describes the amplitude of the vertical oscillations (e.g. Boeche et al. 2013). The e - Z_{max} plane combined with metallicity allows us to characterize the orbits of our HiVel stars while also considering the chemical distribution. Our HiVel sample has median e of 0.73 and median Z_{max} of 13 kpc, which is kinematically consistent with the halo population. This result confirms the assumptions of older works (e.g. Schuster & Nissen 1988; Ryan & Smith 2003; Schuster et al. 2006) that HiVel stars in the solar vicinity mostly belong to the halo. We note that while our specified Galactic potential is thought to be an adequate assumption lo-

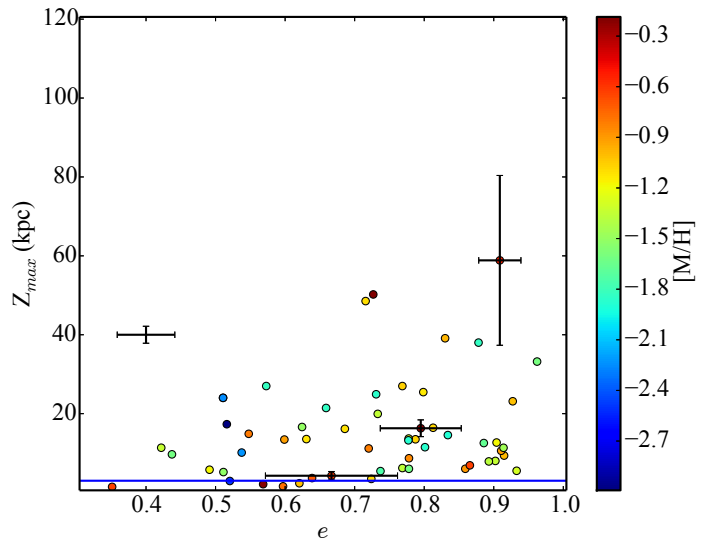


Figure 5. Eccentricity, e , as a function of the maximum Galactic plane height obtained by our HiVel stars during a 1 Gyr orbital integration. The color of each star represents its metallicity, $[M/H]$. The solid horizontal line represents the edge Z_{max} of the thick disk, $Z = 3 \text{ kpc}$ (Carollo et al. 2010). The error bar to the left represents the median uncertainty in both parameters. The other three error bars in e and Z_{max} are shown for the stars with the largest errors on distances. This plot excludes HVS candidates. The high Z_{max} and e for most of the HiVel stars indicate they are consistent with the Galactic halo.

cally, the potential at large distances from the Sun can be relatively uncertain. Since HiVel stars can probe these distant regimes the uncertainties in the orbital parameters, namely the Z_{max} , r_{ap} and r_{per} , are probably underestimated as we only quote the uncertainties by propagating the errors on the observables. There are a few stars with $Z_{max} \lesssim 3 \text{ kpc}$ and eccentricities below 0.6. These stars could be interpreted as thick-disk contaminants especially given their relatively high (> -0.90 dex) metallicities (Boeche et al. 2013; Kor-dopatis et al. 2013b,c).

3.2 Chemical Distribution of High-Velocity Stars

The kinematics of our HiVel sample (Section 3.1) indicate these stars are drawn from the halo population and thus they should also have a chemical fingerprint that is consistent with the halo. In Figure 6 we compare the normalized metallicity distribution of the RAVE and HiVel samples. It is clear that the mean metallicity of the RAVE sample ($\langle [M/H] \rangle_{\text{RAVE}} = -0.22$ dex) is significantly higher than mean metallicity of the HiVel sample ($\langle [M/H] \rangle_{\text{HiVel}} \sim -1.2$ dex). The mean metallicity of our HiVel sample is slightly higher but consistent within the errors with the inner Galactic halo, which is thought to have a mean metallicity around -1.60 dex (Carollo et al. 2007, 2010). The inner Galactic halo is also thought to have measurable α -enhancement (Nissen & Schuster 2010; Haywood et al. 2013; Boeche et al. 2013).

The distribution in $[\alpha/\text{Fe}]$ space will provide information on the birthplace of the stars. Many recent surveys have shown that the different components of the Galaxy can be partially separated in $[\alpha/\text{Fe}]$ - metallicity space (Nissen & Schuster 1997; Fulbright 2002; Stephens & Boesgaard 2002; Nissen & Schuster 2010; Ruchti et al. 2010; Nissen & Schuster 2012; Haywood et al. 2013;

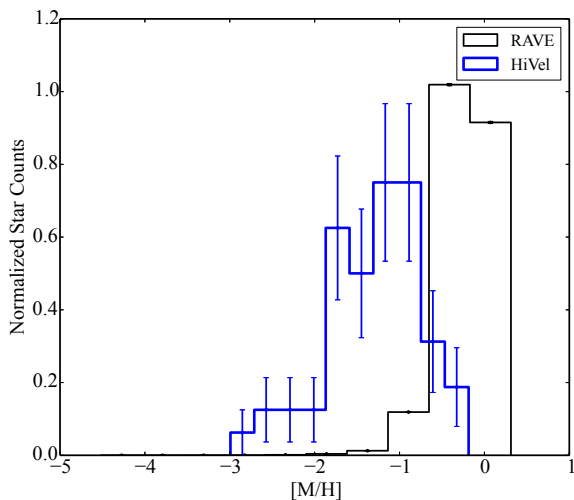


Figure 6. $[M/H]$ distribution for the RAVE catalogue (black) and the HiVel sample (blue). The HiVel stars in our sample are significantly more metal-poor compared to the RAVE mother sample. The peak of the metallicity distribution of HiVel stars is -1.18 dex and is consistent with the Galactic halo. The error bars are computed assuming Poisson noise.

Feltzing & Chiba 2013). These studies show a relationship between the metallicity and $[\alpha/Fe]$ that is described in section 2.1.

For comparison, we plot our HiVel stars in this space relative to the full RAVE sample along with the expected Galactic trend (see Figure 7). The expected uncertainty in both $[M/H]$ and $[\alpha/Fe]$ is $\sim \pm 0.2$ dex (Kordopatis et al. 2013a). Further, we can see from Figure 8 that our HiVel star sample is slightly α -enriched, with a mean α -abundance of $[\alpha/Fe]_{HiVel} = +0.24$ dex, compared to the RAVE mother sample, with a mean α -abundance of $[\alpha/Fe]_{RAVE} = +0.14$ dex. This result is, within the errors, chemically consistent with the halo population. The large dispersion (on the order of 0.25 dex) in the $[\alpha/Fe]$ is likely a result of the uncertainty of the individual $[\alpha/Fe]$ estimates, but may also represent an α -poor and α -enriched population in our HiVel sample. The large uncertainty in the $[\alpha/Fe]$ estimates, particularly at low metallicity, is a result of insufficient spectral information on the abundance of α -elements in the part of the spectrum covered by RAVE (Kordopatis et al. 2013a).

Combining the kinematic and chemical properties, we plot the 2-dimensional density of the GRV as a function of metallicity for the RAVE sample and our HiVel stars (red squares) in Figure 9. Viewing the results in this space allows us to identify clearly one star, J2217 that has an extremely high GRV (~ 360 km s^{-1}), but paradoxically is metal-rich ($[M/H] = -0.18 \pm 0.08$ dex). This star is an outlier compared to the rest of the metal-poor HiVel stars of our sample. If we make a simplistic assumption that the (inner) Galactic stellar halo metallicity distribution function can be modeled as a Gaussian with a mean of $[M/H] = -1.50$ dex and $\sigma_{[M/H]} = 0.50$ (Chiba & Beers 2000), the probability of drawing a star of that metallicity is 0.4 per cent (2.64σ). Assuming higher mean and dispersion values, $(-1.20, 0.54)$, see Kordopatis et al. 2013b) the probability of drawing a star of that metallicity is 2.9 per cent (1.89σ). In either case, the probability of drawing a star of this metallicity from the Galactic halo population is small (< 4 per cent Carollo et al. 2007, 2010; Kordopatis et al. 2013b; An et al. 2013). This star provides us with a unique opportunity to explore metal-rich

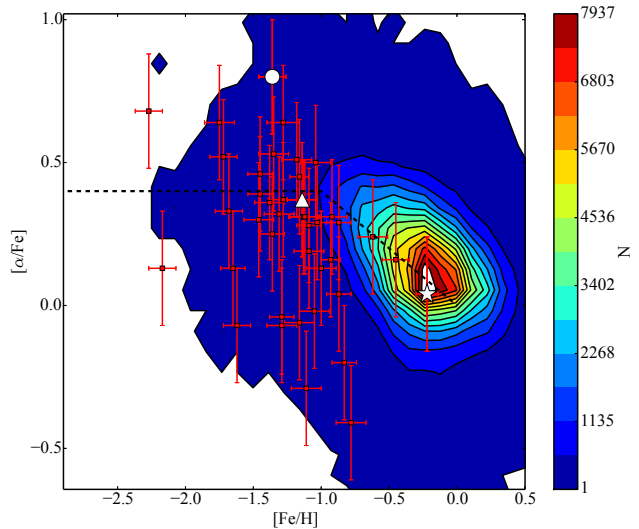


Figure 7. Contour plot showing the $[\alpha/Fe]$ - $[Fe/H]$ for RAVE including where the HiVel stars (red squares) fall in this space. The dotted black line represents the standard Galactic trend in this space. Most of our HiVel stars are, within the errors consistent with the halo population with $[Fe/H]$ less than -1.0 dex and noticeable α -enrichment. The open circle, star and triangle are the same as in Figure 1.

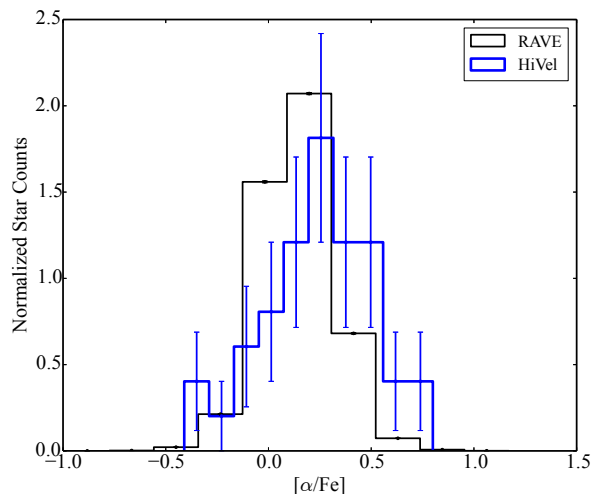


Figure 8. $[\alpha/Fe]$ distribution for the RAVE catalogue (black) and the HiVel sample (blue). The HiVel sample is slightly more α -enriched compared to the RAVE mother sample but the dispersions are comparable.

halo stars. As such, the next section is devoted to exploring this object in more detail.

It is worth mentioning there are two additional stars that have $[M/H]$ larger than -0.50 dex which are classified as HiVel stars. J152905.9-365544 is a giant star which has a GRV = -276 ± 1.5 km s^{-1} with a metallicity of $[M/H] = -0.21 \pm 0.1$ dex and $[\alpha/Fe] \sim +0.16 \pm 0.2$ dex. On the Toomre diagram (Figure 4), this star sits just above the thick disk region. An orbital integration of this star was performed and showed that this star has an $e \sim 0.5$ with $Z_{max} \sim 3 \pm 1$ kpc. Using the same probabilistic kinematic classification from Bensby, Feltzing & Lundström (2003) this star would be categorized as a thick disk star. Given the kinematic and

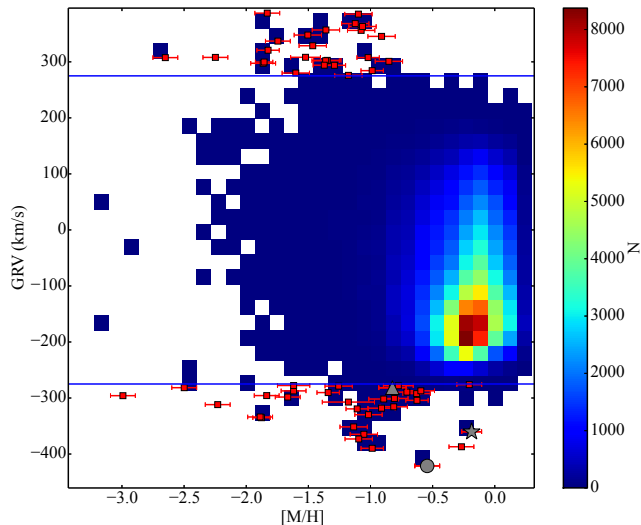


Figure 9. 2D density plot of the GRV and $[M/H]$ for the RAVE sample. The horizontal lines indicate the adopted kinematic minimum kinematic GRV needed to be classified as a HiVel candidate (i.e. absolute GRV $> 275 \text{ km s}^{-1}$). It is interesting to note that there are three HiVel stars with relatively high metallicities ($[M/H]$ larger than -0.5 dex). The gray circle, star and triangle are the same as in Figure 1.

chemical properties of this star, we expect it is a thick disk contaminate. The second star, J193647.0-590741, has an estimated metallicity of $[M/H] = -0.27 \pm 0.1$ dex, yet kinematically it has a GRV = $-387 \pm 1.7 \text{ km s}^{-1}$. Orbital integration for this star indicates it has an $e \sim 0.82$ with $Z_{max} \sim 16 \pm 5 \text{ kpc}$ which resembles halo-like properties. While the stellar parameter pipeline is able to estimate its T_{eff} , $\log g$ and $[M/H]$, the chemical pipeline fails to provide an estimate of the $[Fe/H]$ and $[\alpha/Fe]$. This could be due to the low SNR (~ 20) and thus high-resolution, high SNR follow-up will be necessary to confirm the chemical signature of this star.

3.3 Captured Star or High-Velocity Ejected Disk Star?: The Case of J2217

The giant star J2217 represents an unusually fast-moving object with a metallicity significantly above -1.0 dex. The RAVE stellar parameter pipeline has estimated it to have a $T_{\text{eff}} = 4790 \pm 80 \text{ K}$ and $\log g = 2.05 \pm 0.15$ dex. It has a metallicity of -0.18 ± 0.1 dex (at a SNR = 71.0) and an $[\alpha/Fe] = +0.04 \pm 0.2$ dex. The chemistry of this star, particularly the high metallicity and low levels of α -enhancement, is consistent with a disk or possibly captured star but not the Galactic halo like most of the other HiVel stars. We have no reason to believe this star is a member of a binary star based on the ‘normal’ spectral morphological classification of Matijević et al. (2012) and is classified as a single normal star in the UCAC4 catalogue (Zacharias et al. 2013).

Kinematically, the star is in the extreme halo region residing below the HVS boundary on the Toomre Diagram (Figure 4). The total Galactic rest frame velocity of this star is $426 \pm 10 \text{ km s}^{-1}$. The Tonry-Davis correlation coefficient estimated by RAVE is 65 indicating the template for cross-correlation was a good fit and the uncertainty in the measured RV approximately 1 km s^{-1} . This puts it $\sim 100 \text{ km s}^{-1}$ below the Galactic escape speed of Piffl et al. (2014) at its Galactocentric distance of $r = 8.01 \pm 0.13 \text{ kpc}$. To better understand the kinematics of this object we integrated its orbit

over 1 Gyr (Figure 13) to get an idea of the shape of the orbit without being dominated by errors due to the observables. We found that J2217 reaches a $Z_{max} = 31 \pm 5 \text{ kpc}$ and has an overall eccentricity of $e = 0.72 \pm 0.02$. This star kinematically resembles a halo star given its Z_{max} (e.g. Coşkunoğlu et al. 2012) and eccentricity yet its chemistry suggests it may belong to the Galactic disk or a dwarf galaxy (e.g. Sheffield et al. 2012).

The orbital integration described above was used to estimate the time-of-flight (TOF) for this star assuming it was produced in the Galactic disk and ejected into the halo (Figure 13). The star is passing through the disk and the TOF required to get the star near the galactic disk again ($|z| < 3 \text{ kpc}$) is $\sim 600 \text{ Myr}$ well within the lifetime of a low-mass star. Bromley et al. (2009) argued that the metal-rich tail of the (inner) halo metallicity distribution may come from stars born in the disk and kinematically heated (by binary supernova ejection) into the halo as ejected disk stars. In terms of the time-scale, kinematics, and chemistry it is perfectly reasonable this object was born in the Galactic disk and was kinematically heated, maybe as a result of binary ejection or tidal interactions with satellite galaxies as in Purcell, Bullock & Kazantzidis (2010) or other gravitational means, causing it to be now observed as a part of the Galactic halo. Alternatively, this star could be a captured star from a dwarf spheroidal galaxy. Reaching out to a vertical distance of 35 kpc is within the distance of a couple massive dwarf galaxies (e.g. Sagittarius dwarf galaxy). Chemically, massive dwarf galaxies like the Sagittarius dwarf spheroidal galaxy may contain some stars as metal-rich as $[M/H] = -0.20$ dex with a depletion in $[\alpha/Fe] \sim -0.20$ dex (Sbordone et al. 2007). J2217 is metal-rich with no noticeable enhancement in $[\alpha/Fe]$ (i.e. an $[\alpha/Fe] = -0.20$ dex is at the edge of the ± 0.2 dex error budget for the $[\alpha/Fe]$ estimate. However, given that the 3 dimensional velocity vector of this star indicates that it is currently on its way out of the Galaxy and chemically resembles the Galactic disk, it is more likely this star is an ejected disk star.

We observed J2217 in high-resolution (black line in Figure 10) using the APO to try determining whether the star is captured or ejected. The analysis of the high-resolution spectra (described in Section 2.2) yielded stellar parameters ($T_{\text{eff}} = 4635 \pm 77 \text{ K}$, $\log g = 2.06 \pm 0.20$ dex, and $[Fe/H] = -0.21 \pm 0.13$ dex, HRV = $-490.8 \pm 0.8 \text{ km s}^{-1}$) that are in very good agreement with those found in RAVE DR4. The confirmation of the impressively high metallicity for this HiVel star indicates that it is unlikely to have come from a dwarf galaxy that, on average, have significantly lower metallicities. The results of the abundance pattern in the α -elements (Figure 11(a)) and neutron-capture elements (Figure 11(b)), of J2217 can be found in Figure 11 and correspondingly in Table 1. We also explored the Na-Ni abundances of J2217 in Figure 12. Studies as early as Nissen & Schuster (1997) indicated that $[Na/Fe]$ and $[Ni/Fe]$ may distinguish stars that were accreted from other field population stars. Exploring this relationship between Ni-Na will allow us to determine if J2217 is consistent with having been accreted. We found that the abundance pattern of J2217 namely the α -elements, neutron-capture elements, and the abundance ratios of $[O/Fe]$, $[Ni/Fe]$, $[Al/Fe]$, and $[Na/Fe]$, most resembles the Galactic (thick) disk. It is worth mentioning that we found a relatively high enhancement in Barium, $[Ba/Fe] = +0.35$ dex, for J2217 however it is still within the range of the thick disk. Furthermore, the abundances in Table 1, namely Fe, Na, and O, were compared with known globular clusters (e.g. Carretta et al. 2009) to determine if this star is consistent with a metal-rich globular cluster. This test indicated that J2217 is not consistent with any known globular clusters.

When we couple the abundance analysis with that of the

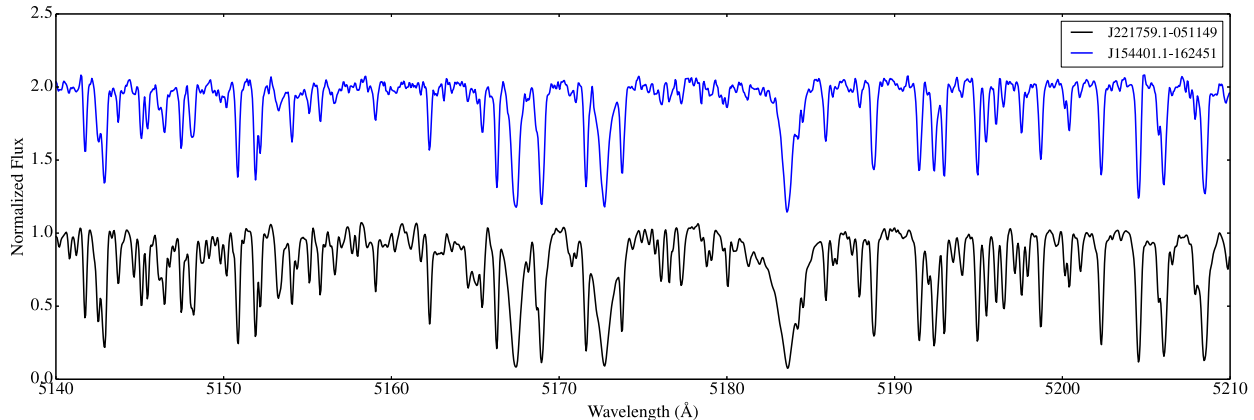


Figure 10. The observed high-resolution ACRES spectrum of the giant star J2217 (black line) and J1544 (blue line) in the Mg I triplet region. In both cases these spectra were used to determine the chemical abundances which are shown in Table 1 and Table 2.

Table 1. ARCES Elemental Abundances for J2217

Species	N	$\log \epsilon (X)$	σ	[X/Fe]
Mg	8	7.56	0.14	+0.25
Ca	6	6.32	0.04	+0.23
Ti I	4	4.91	0.04	+0.23
Ti II	5	4.75	0.13	+0.07
Si	8	7.42	0.10	+0.13
C I	5	8.33	0.05	+0.16
O	1	8.69	0.10	+0.25
Fe I	60	7.23	0.13	...
Fe II	8	7.22	0.08	...
Al	3	6.43	0.03	+0.28
Na	5	6.17	0.09	+0.22
Ni	5	6.15	0.09	+0.14
Ba II	3	2.30	0.04	+0.35
La II	6	0.93	0.06	+0.02
Zr II	3	2.19	0.07	-0.18
Sr I	1	2.73	0.10	+0.03
Eu II	2	0.40	0.02	-0.19
Cu I	3	3.78	0.10	-0.21

NOTE: The chemical abundances of each species (column 1) are shown. Column 2 is the number of lines used to determine the abundance of each species. Column 3 is the log of the absolute abundance and the line-to-line dispersion is listed in column 4. Where there is only one line we quote a conservative error bar of ± 0.10 dex. Finally, column 5 is the solar relative abundances.

orbital integration we favor a scenario in which this star was kicked out of the Galactic (thick) disk. The mechanism by which this star was ejected from the disk, namely dwarf galaxy heating (Purcell, Bullock & Kazantidis 2010), binary supernova ejection (Bromley et al. 2009) or other gravitational mechanisms, is unclear. Regardless, this provides observational support for the idea that the most metal-rich stars in the Galactic halo may have been assembled by kicking out Galactic disk stars (Bromley et al. 2009).

3.4 Hypervelocity Star Candidates

HVSs are rare fast-moving stars which have velocities that exceed the Galactic escape speed ($\sim 533 \text{ km s}^{-1}$ at the solar circle, Piffl

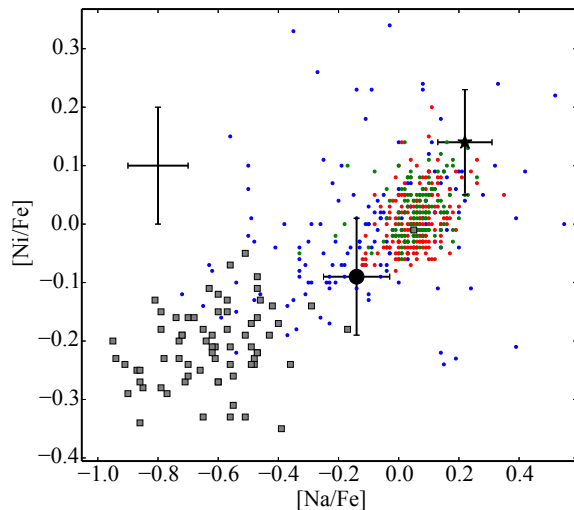


Figure 12. The observed high-resolution abundances of Ni as a function of Na for J2217 (black star) and J1544 (black circle). The symbols are the same as Figure 11. We find that J2217 is chemically consistent with the disk and not a dwarf galaxy (such as the Fornax). However it is possible that J1544, within the errors, may be consistent with a massive dwarf galaxy. The error bars on the side represent the mean error of the abundances from the literature.

et al. 2014). Recent studies have used HVSs to better understand conditions and dynamics of the hidden Galactic Centre as well as the Galactic halo (Kollmeier et al. 2010; Brown, Geller & Kenyon 2009).

We have identified one HVS candidate whose galactic rest-frame velocity is more than $1\text{-}\sigma$ above the escape speed and three stars whose velocities, within the uncertainties, are above 500 km s^{-1} that are worth additional scrutiny. Their basic observational and kinematical properties can be found in Table 3 and Table 4, respectively. J1610 has a metallicity of -0.86 dex and is at a Galactocentric radius of approximately 5 kpc and has a V_{GRF} of $807 \pm 154 \text{ km s}^{-1}$. Assuming the escape speed of Piffl et al. (2014) at this radius ($\sim 600 \text{ km s}^{-1}$), this candidate has a velocity at least $1\text{-}\sigma$ above the escape speed and is among the first HVS candidates

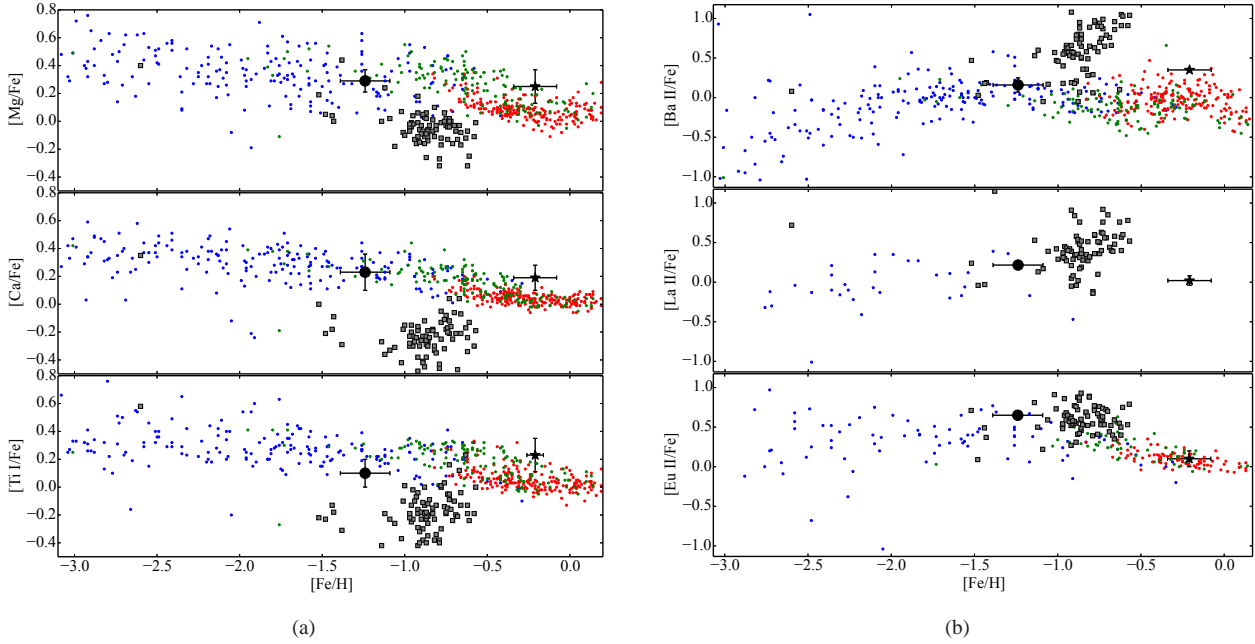


Figure 11. (a) The abundance patterns of the α -elements as a function of metallicity including [Mg/Fe], [Ca/Fe] and [Ti/Fe] from top to bottom, respectively for J2217 (black star) and J1544 (black circle). (b) The abundance patterns of neutron-capture elements as a function of metallicity including [Ba II/Fe], [La II/Fe], and [Eu/Fe] from top to bottom respectively. The small coloured circles represent abundances of thin disk (red), thick disk (green) and halo (blue) stars from Venn et al. (2004). For comparison, the grey squares show an example of a dwarf galaxy (Fornax) from Letarte et al. (2010). J2217 is chemically consistent in the α -elements and most neutron-capture elements with the Galactic thick disk. On the other hand J1544 is chemically consistent with the halo field population or dwarf galaxies. The error bars on the side represent the mean error of the abundances from the literature.

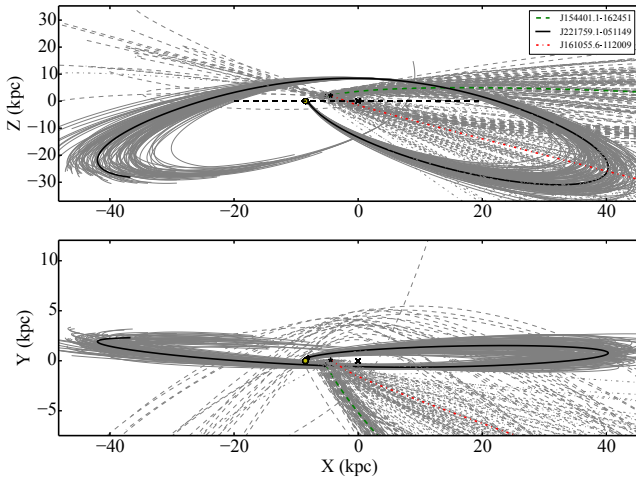


Figure 13. A 1 Gyr orbital integration for J2217 (black solid line), J1544 (green dotted line), and J1610 (red dash-dotted line). The yellow circle represents the Sun, the black 'x' represents the Galactic center and the black asterisk represents the current position of J2217 and J1544. The thin grey lines are 100 draws of the orbital integration to illustrate the uncertainty. We find that both stars are currently passing through the disk.

from RAVE. If the escape speed were significantly higher, above 650 km s^{-1} , this candidate would have a velocity less than $1\text{-}\sigma$ escape speed but still impressively high. It is important to note there is relatively bright star close to this star and thus the uncertainties in the proper motion may be underestimated. More accurate distance

and proper motion estimates will help decrease the error in order to confirm the total space velocity of this target.

To date, the tens of known HVSs are massive ($3\text{--}4 M_{\odot}$) early-type main sequence stars, including hot O, B, and A type stars (Brown, Geller & Kenyon 2009, 2012, 2014). Li et al. (2012) and Palladino et al. (2014) have recently identified potential later-type HVS candidates which still need confirmation. The HVS candidate J1610 is among the few that are not early-type stars. Orbital integration of this HVS candidate indicates that it does not originate in the Galactic Centre. If confirmed, this would add to an increasing list of candidate HVS that do not seem to originate in the Galactic Centre (e.g. Palladino et al. 2014) and thus need an alternative production mechanism (e.g. Yu & Tremaine 2003; Abadi, Navarro & Steinmetz 2009; Heber et al. 2008; Przybilla et al. 2008).

The second star, J1544, has a V_{GRF} of $523 \pm 40 \text{ km s}^{-1}$. This star has a velocity that is just below the escape speed at its position (which is expected to be $\sim 570 \text{ km s}^{-1}$). We have followed up J1544 with high-resolution echelle spectra from the ARCES instrument in order to obtain detailed abundances in part because its high global metallicity ($[M/H] = -0.54$ dex). The spectrum of J1544 in the Mg I triplet region can be found in Figure 10. The stellar parameters of the star was determined using the high-resolution spectra and indicate that J1544 has a $T_{\text{eff}} = 4458 \pm 120 \text{ K}$; $\log g = 1.44 \pm 0.2$ dex; $[\text{Fe}/\text{H}] = -1.24 \pm 0.15$ dex; $\xi = 1.77 \pm 0.06 \text{ km s}^{-1}$ which is consistent with the RAVE parameters. Furthermore, we have confirmed the very high heliocentric RV ($-406.7 \pm 0.80 \text{ km s}^{-1}$) observed by RAVE for this star. Using the stellar parameters, we have determined the abundance of several α and neutron-capture elements. Table 2 contains the high-resolution abundance analysis for J1544 including the species, number of lines used, log of the absolute abundance, the uncertainty (which was estimated as the stan-

Table 2. ARCEN Elemental Abundances for J1544

Species	N	$\log \epsilon (X)$	σ	[X/Fe]
Mg	5	6.58	0.08	+0.29
Ca	8	5.30	0.13	+0.23
Ti I	5	3.76	0.09	+0.10
Ti II	1	3.74	0.10	+0.08
Si	7	6.50	0.06	+0.23
Al I	3	5.33	0.05	+0.20
Na I	5	4.79	0.11	-0.14
Ni I	5	4.90	0.10	-0.09
Fe I	95	6.21	0.15	...
Fe II	16	6.23	0.16	...
Ba II	3	1.11	0.09	+0.16
La II	5	0.13	0.04	+0.22
Eu II	2	-0.05	0.04	+0.65

NOTE: The format is the same as in Table 1.

dard deviation of the abundance determined from each individual line), and the solar-scaled abundance ratio. The $[\alpha/\text{Fe}]$ for this star was determined by computing the mean abundance of the four α -elements including Mg, Ca, Ti, and Si.

The high-resolution abundances for the α -elements (Figure 11(a)) indicates that this star has a small enhancement with an $[\alpha/\text{Fe}] = +0.21 \pm 0.07$ dex. At this metallicity, the star would be classified as one of the ‘low- α ’ stars of Nissen & Schuster (2010) which they interpret as an ‘accreted’ population. The neutron-capture elemental abundances of J1544 is consistent with both the field population and a dwarf galaxy like the Fornax (Figure 11(b)). The Al and Mg ratios, $[\text{Al}/\text{Fe}] = +0.20 \pm 0.05$ and $[\text{Mg}/\text{Fe}] = +0.29 \pm 0.08$ dex respectively, are consistent with the field population (Fulbright 2002). The abundance of $[\text{Na}/\text{Fe}]$ and $[\text{Ni}/\text{Fe}]$ are both depleted (Figure 12). Within the errors, the Na-Ni of this star is consistent with both the field star population of Venn et al. (2004) and Nissen & Schuster (2011) and massive dwarf galaxies. The chemical information from the high-resolution analysis indicates that this star is not consistent with the Galactic thin disk, because its metallicity is too low. The star also does not likely originate in the Galactic thick disk as one would expect a higher α -abundance. We also compared the abundances of this star to known globular clusters with similar iron abundances (e.g. Carretta et al. 2009). The depletion in Na and Ni combined with the abundances of Al and Mg do not seem consistent with globular clusters. Its chemistry suggests that this star may have a halo or dwarf galaxy formation site.

It is also worth mentioning that in addition to the HVS candidate there are two other extremely high velocity bound stars whose total velocity vectors are at or near 500 km s^{-1} . Namely, J142103.5-374549 has a $v_{GRF} = 460 \pm 70 \text{ km s}^{-1}$ and J155304.7-060620 has a $v_{GRF} = 474 \pm 43 \text{ km s}^{-1}$. Orbital integration shows J142103.5-374549 is on a highly elliptical orbit ($e = 0.91$) getting as close as 3.72 kpc to the Galactic Centre. We note that J142103.5-374549 was excluded from Piffil et al. (2014) because of its unusual place on the Hertzsprung-Russell diagram. Further, both J142103.5-374549 and J155304.7-060620 have conflicting distance, and proper motions when comparing UCAC4 and distances from Binney et al. (2014a) with those of Bilir et al. (2012) and Francis (2013).

4 DISCUSSION AND CONCLUSION

We have aimed to characterize a set of HiVel stars in RAVE DR4. To do this, we applied a series of quality cuts on the initial RAVE DR4 ensuring the data have quality spectra and measurements needed to estimate the 6D position and velocity vector as well as estimates of metallicity. In order to maximize the HiVel stars in our sample, we selected stars which have absolute galactic-rest frame RVs (corrected for solar motion) $> 275 \text{ km s}^{-1}$. This led to some contamination from disk stars near $l = 90^\circ$ and 270° where the primary component of the disk stars velocity is along the line-of-sight. To deselect these stars, we made a stricter cut in GRV within $\pm 50^\circ$ of the above Galactic latitudes. We sourced the distances from the estimated spectrophotometric parallaxes from Binney et al. (2014a) and proper motions from the UCAC4 catalogue (Zacharias et al. 2013) and combined it with the information from RAVE DR4 to obtain the full 6D position and velocity vectors. We also implemented an orbital integration code to determine orbital parameters, particularly Z_{max} and eccentricity, to study the kinematics. We also studied the metallicity and $[\alpha/\text{Fe}]$ abundances that compliment the kinematical study of our sample by attempting to measure the chemical distribution of our HiVel stars.

Our results can be summarized in the following way:

(i) Kinematically, HiVel stars are mostly consistent with the Galactic halo (Figure 4) and are characterized by eccentric orbits that can extend, on average, 14 kpc out of the Galactic plane. Chemically, HiVel stars in RAVE are metal-poor (peaking at $[\text{M}/\text{H}] = -1.2$ dex) compared to the rest of RAVE (peaking $[\text{M}/\text{H}] = -0.22$ dex), which is consistent with the (inner) halo (Kordopatis et al. 2013b; Carollo et al. 2007, 2010; Piffil et al. 2014). While the metal-weak thick disk overlaps the metallicity region of the HiVel stars, the rather hot kinematics that describe the HiVel stars (Figure 5) favors the Galactic halo as a current location. It is interesting to point out that the mean iron abundance of the inner Galactic halo from Carollo et al. (2007) is slightly more metal-poor compared to the mean *global metallicity* of our HiVel stars.

(ii) The HiVel stars in our sample are, on average, α -enhanced compared to the rest of the RAVE sample (Figure 8). The $[\alpha/\text{Fe}]$ distribution of the HiVel stars is consistent, within the $1\text{-}\sigma$ error, to the α -enhancement ($[\alpha/\text{Fe}] \sim +0.4$) expected of inner halo stars (Haywood et al. 2013; Nissen & Schuster 2012, 2010; Ruchti et al. 2010; Adibekyan et al. 2012; Sheffield et al. 2012). The inner halo is thought to be formed of two components: an α -rich component maybe formed in situ and an α -poor component possibly accreted by dwarf galaxies (Nissen & Schuster 2010; Schuster et al. 2012; Hawkins et al. 2014). The large spread in α -enrichment of the both RAVE (~ 0.18 dex) and HiVel stars (~ 0.25 dex) in our sample could be suggestive of an α -rich and α -poor population in both samples. However, it is more likely that this is blurred by the uncertainty in the $[\alpha/\text{Fe}]$ estimates from the chemical pipeline of the RAVE DR4 (Boeche et al. 2011; Kordopatis et al. 2013a).

(iii) While most of the HiVel stars are metal-poor, there are several stars that have metallicity above -1.0 dex. These stars, while having kinematics that resemble halo stars, have disk like metallicity and thus do not conform to the rest of HiVel stars. One of these stars, J2217 has a particular high metallicity ($[\text{M}/\text{H}] = -0.18$). Depending on how one defines the metallicity distribution function in the halo this star is a $\sim 1.9\text{-}4\sigma$ outlier (An et al. 2013; Carollo et al. 2007, 2010; Kordopatis et al. 2013b; Chiba & Beers 2000). Conversely, we can assess the probability this star being kinematically apart of the thin disk, thick disk, or halo. This star is described by an orbit with a $Z_{max} = 35 \pm 10$ kpc, overall eccentricity of $e = 0.72 \pm$

Table 3. Observational Properties of HVS and Metal-Rich HiVel Star Candidates

RAVEID	α ($^{\circ}$)	δ ($^{\circ}$)	$\mu_{\alpha} \cos(\delta)$ (mas/yr)	$\sigma\mu_{\alpha} \cos(\delta)$ (mas/yr)	μ_{δ} (mas/yr)	$\sigma\mu_{\delta}$ (mas/yr)	d_{\odot} (pc)	σd_{\odot} (pc)	[M/H] (dex)	[α /Fe] (dex)
J155304.7-060620	238.26967	-6.10550	-28.0	1.3	26.9	1.3	1480	463	-1.67	0.33
J142103.5-374549	215.26442	-37.76361	8.7	1.4	3.1	1.4	3963	2541	-1.60	0.50
J154401.1-162451	236.00438	-16.41428	2.6	2.2	3.8	2.6	3544	1222	-0.54	0.80
J161055.6-112009	242.73183	-11.33589	-25.6	2.2	22.9	2.4	4369	1451	-0.82	0.37
J152905.9-365544	232.27450	-36.92883	-4.8	2.0	3.4	2.0	2863	738	-0.21	0.16
J193647.0-590741	294.19575	-59.12814	3.5	1.1	-8.4	2.2	618	301	-0.27	...
J221759.1-051149	334.49604	-5.19700	-20.4	1.1	5.0	1.1	580	147	-0.18	0.04

Table 4. Kinematic Properties of HVS and Metal-Rich HiVel Star Candidates

RAVEID	HRV (km s^{-1})	σ HRV (km s^{-1})	U (km s^{-1})	σ U (km s^{-1})	V (km s^{-1})	σ V (km s^{-1})	W (km s^{-1})	σ W (km s^{-1})	V_{GRF} (km s^{-1})	σV_{GRF} (km s^{-1})
J155304.7-060620	-317.9	0.9	-408	46	235	10	47	66	473	47
J142103.5-374549	405.2	1.1	413	76	136	96	151	29	460	73
J154401.1-162451	-403.2	1.7	-335	21	358	48	-179	37	522	29
J161055.6-112009	-296.8	1.0	-589	112	249	50	492	209	807	159
J152905.9-365544	-189.8	1.5	-186	15	296	24	26	33	351	17
J193647.0-590741	-314.0	1.8	-261	8	317	12	146	6	436	8
J221759.1-051149	-491.0	0.9	-133	10	-23	6	404	9	426	8

0.03, and a Galactic rest frame velocity of $426 \pm 10 \text{ km s}^{-1}$ (consistent with the Galactic halo). Using the population classification from the full space motion described in [Bensby, Feltzing & Lundström \(2003\)](#), we found this particular giant star is classified as a ‘high-probability’ halo star. [Ivezić et al. \(2008\)](#) found that while the metallicity distribution of the inner halo peaks at -1.2 dex, the tail of the distribution extends up to approximately solar metallicities. Theoretically, [Bromley et al. \(2009\)](#) discusses the possibility of runaway disk stars being a contributor to the high-metallicity tail of the inner stellar halo. Could this star be observational evidence of this conjecture?

To help answer this, we obtained high-resolution spectrum J2217 (Figure 10) to do detailed chemical abundance analysis. We confirmed the stellar parameters of RAVE and measured the abundances of light elements, α -elements and neutron-capture elements, which can be found in Table 1. The abundances (see Figure 11 and Figure 12) and the orbital integration (see Figure 13) of J2217 confirm that this star was likely born in the Galactic thick disk. The abundances of Fe, Na, and O are not consistent with known globular clusters (e.g. [Carretta et al. 2009](#)). Given the lack of s-process enhancement, or other chemical peculiarities, it is likely this star was kicked into the Galactic halo via gravitation mechanisms. Alternatively, given that nearly half of solar-type stars are in binary systems ([Duchêne & Kraus 2013](#)), this star could also have been launched into the halo by a binary disruption event. The lack of neutron-capture and carbon enhancement however could point to the former scenario. The discovery of this runaway disk star indicates that while almost all HiVel stars currently reside in the Galactic halo, they were not necessarily *born* in the halo.

(iv) We have found a HVS candidate using RAVE whose total Galactic rest frame velocity is larger the expected escape velocity (above the 1- σ level). The HVS candidate is an evolved giant which is different than the known B-type HVS that are currently discussed in the literature (e.g. [Brown, Geller & Kenyon 2014, 2009](#)).

(v) We also followed up the star with the second highest veloc-

ity (with V_{GRF} larger than 500 km s^{-1}) in our sample (J1544). We confirmed the stellar parameters determined by RAVE of this star as well as measured abundance of several α -elements, neutron-capture elements. The chemical abundances, found in Table 2, are consistent with either the halo field star origin or (massive) dwarf galaxy origin (see Figure 11 and Figure 12). The high speed, total Galactic rest frame velocity of $526 \pm 40 \text{ km s}^{-1}$, is near but not above the Milky Way escape speed at its position and is unusually fast for a halo field star. Furthermore, the orbital integration indicates this object is currently passing through the disk (Figure 13). While it may be possible for this star to be born in the halo and achieve such a high velocity it is also possible that the star has been accreted from a dwarf galaxy (e.g. [Abadi, Navarro & Steinmetz 2009](#); [Piffl, Williams & Steinmetz 2011](#)) and may explain its velocity near the escape speed. The chemodynamics of this particular star is consistent with either scenario leaving its origins unknown.

It is interesting to study the chemistry and kinematics together of the HVS and HiVel star candidates as they give us invaluable information about the formation environment of these populations. Our analysis has shown that HVS that are near the Galactic escape speed should have complimenting chemical information to better constrain its formation environment. [Palladino et al. \(2014\)](#) has found a set of 20 metal-poor HVS candidates with SDSS of those 6 have velocities within 100 km s^{-1} of the escape speed assuming spherical potential. Could these be captured stars as well? Complementary chemical abundance analysis may help decipher where these stars originate from and thus shed light on potential formation mechanisms for HVS. With the upcoming Gaia mission, we will better be able to constrain the distances, proper motions and thus the total velocity vector for all of our stars but more specifically the HVS candidates.

ACKNOWLEDGEMENTS

We would like to thank the anonymous referee whose comments improved this manuscript. We also would like to thank P. Jofré, A. Casey, and V. Belokurov for discussions that greatly improved this work. K.H. is funded by the British Marshall Scholarship program and the King's College, Cambridge Studentship. R. F. G. W. acknowledges funding from the NSF grant OIA-1124403. This work is based on observations obtained with the Apache Point Observatory 3.5-meter telescope, which is owned and operated by the Astrophysical Research Consortium. Funding for RAVE has been provided by: the Australian Astronomical Observatory; the Leibniz-Institut fuer Astrophysik Potsdam (AIP); the Australian National University; the Australian Research Council; the French National Research Agency; the German Research Foundation (SPP 1177 and SFB 881); the European Research Council (ERC-StG 240271 Galactica); the Istituto Nazionale di Astrofisica at Padova; The Johns Hopkins University; the National Science Foundation of the USA (AST-0908326); the W. M. Keck foundation; the Macquarie University; the Netherlands Research School for Astronomy; the Natural Sciences and Engineering Research Council of Canada; the Slovenian Research Agency; the Swiss National Science Foundation; the Science & Technology Facilities Council of the UK; Opticon; Strasbourg Observatory; and the Universities of Groningen, Heidelberg and Sydney. The RAVE web site is at <http://www.rave-survey.org>

REFERENCES

- Abadi M. G., Navarro J. F., Steinmetz M., 2009, *ApJLett*, 691, L63
- Adibekyan V. Z., Sousa S. G., Santos N. C., Delgado Mena E., González Hernández J. I., Israelian G., Mayor M., Khachatryan G., 2012, *A&A*, 545, A32
- Alvarez R., Plez B., 1998, *A&A*, 330, 1109
- An D. et al., 2013, *ApJ*, 763, 65
- Bensby T., Feltzing S., Lundström I., 2003, *A&A*, 410, 527
- Bilir S., Karaali S., Ak S., Önal Ö., Dağtekin N. D., Yontan T., Gilmore G., Seabroke G. M., 2012, *MNRAS*, 421, 3362
- Binney J. et al., 2014a, *MNRAS*, 437, 351
- Binney J. et al., 2014b, *MNRAS*, 439, 1231
- Blaauw A., 1961, *Boletin de los Observatorios de Tonantzintla y Tacubaya*, 15, 265
- Boeche C. et al., 2013, *A&A*, 553, A19
- Boeche C. et al., 2011, *AJ*, 142, 193
- Bromley B. C., Kenyon S. J., Brown W. R., Geller M. J., 2009, *ApJ*, 706, 925
- Brown W. R., Geller M. J., Kenyon S. J., 2009, *ApJ*, 690, 1639
- Brown W. R., Geller M. J., Kenyon S. J., 2012, *ApJ*, 751, 55
- Brown W. R., Geller M. J., Kenyon S. J., 2014, *ArXiv e-prints*, arXiv:1401.7342
- Carollo D. et al., 2010, *ApJ*, 712, 692
- Carollo D. et al., 2007, *Nature*, 450, 1020
- Carretta E., Bragaglia A., Gratton R., Lucatello S., 2009, *A&A*, 505, 139
- Chiba M., Beers T. C., 2000, *AJ*, 119, 2843
- Coşkunoğlu B., Ak S., Bilir S., Karaali S., Önal Ö., Yaz E., Gilmore G., Seabroke G. M., 2012, *MNRAS*, 419, 2844
- Duchêne G., Kraus A., 2013, *ARA&A*, 51, 269
- Feltzing S., Chiba M., 2013, *NAR*, 57, 80
- Francis C., 2013, *MNRAS*, 436, 1343
- Fulbright J. P., 2002, *AJ*, 123, 404
- Gratton R. G., Carretta E., Desidera S., Lucatello S., Mazzei P., Barbieri M., 2003, *A&A*, 406, 131
- Gustafsson B., Edvardsson B., Eriksson K., Jørgensen U. G., Nordlund Å., Plez B., 2008, *A&A*, 486, 951
- Hawkins K., Jofré P., Gilmore G., Masseron T., 2014, *MNRAS*, 445, 2575
- Haywood M., Di Matteo P., Lehnert M. D., Katz D., Gómez A., 2013, *A&A*, 560, A109
- Heber U., Edelmann H., Napiwotzki R., Altmann M., Scholz R.-D., 2008, *A&A*, 483, L21
- Hill V. et al., 2002, *A&A*, 387, 560
- Hills J. G., 1988, *Nature*, 331, 687
- Humason M. L., Zwicky F., 1947, *ApJ*, 105, 85
- Ivezić Ž. et al., 2008, *ApJ*, 684, 287
- Johnson D. R. H., Soderblom D. R., 1987, *AJ*, 93, 864
- Johnston K. V., Spergel D. N., Hernquist L., 1995, *ApJ*, 451, 598
- Kollmeier J. A. et al., 2010, *ApJ*, 723, 812
- Kordopatis G. et al., 2013a, *AJ*, 146, 134
- Kordopatis G. et al., 2013b, *MNRAS*, 436, 3231
- Kordopatis G. et al., 2013c, *A&A*, 555, A12
- Kordopatis, G. R. C., 2014, *ArXiv e-prints*, arXiv:1410.4254
- Kupka F., Ryabchikova T. A., 1999, *Publications de l'Observatoire Astronomique de Beograd*, 65, 223
- Letarte B. et al., 2010, *A&A*, 523, A17
- Li Y., Luo A., Zhao G., Lu Y., Ren J., Zuo F., 2012, *ApJLett*, 744, L24
- Löckmann U., Baumgardt H., 2008, *MNRAS*, 384, 323
- Löckmann U., Baumgardt H., Kroupa P., 2008, *ApJLett*, 683, L151
- Lu Y., Yu Q., Lin D. N. C., 2007, *ApJLett*, 666, L89
- Masseron T., 2006, PhD thesis, Observatoire de Paris, France
- Matičević G. et al., 2012, *ApJS*, 200, 14
- Nissen P. E., Schuster W. J., 1997, *A&A*, 326, 751
- Nissen P. E., Schuster W. J., 2010, *A&A*, 511, L10
- Nissen P. E., Schuster W. J., 2011, *A&A*, 530, A15
- Nissen P. E., Schuster W. J., 2012, *A&A*, 543, A28
- Palladino L. E., Schlesinger K. J., Holley-Bockelmann K., Allende Prieto C., Beers T. C., Lee Y. S., Schneider D. P., 2014, *ApJ*, 780, 7
- Piffl T. et al., 2014, *A&A*, 562, A91
- Piffl T., Williams M., Steinmetz M., 2011, *A&A*, 535, A70
- Plez B., 2012, *Turbospectrum: Code for spectral synthesis*. *Astrophysics Source Code Library*
- Portegies Zwart S. F., 2000, *ApJ*, 544, 437
- Portegies Zwart S. F., Baumgardt H., McMillan S. L. W., Makino J., Hut P., Ebisuzaki T., 2006, *ApJ*, 641, 319
- Poveda A., Allen C., Hernández-Alcántara A., 2005, *ApJLett*, 627, L61
- Poveda A., Ruiz J., Allen C., 1967, *Boletin de los Observatorios Tonantzintla y Tacubaya*, 4, 86
- Przybilla N., Nieva M. F., Heber U., Firnstein M., Butler K., Napiwotzki R., Edelmann H., 2008, *A&A*, 480, L37
- Purcell C. W., Bullock J. S., Kazantzidis S., 2010, *MNRAS*, 404, 1711
- Ruchti G. R. et al., 2010, *ApJLett*, 721, L92
- Ryan S. G., Smith I. M., 2003, *MNRAS*, 341, 199
- Sbordone L., Bonifacio P., Buonanno R., Marconi G., Monaco L., Zaggia S., 2007, *A&A*, 465, 815
- Schönrich R., 2012, *MNRAS*, 427, 274
- Schuster W. J., Moitinho A., Márquez A., Parrao L., Covarrubias E., 2006, *A&A*, 445, 939

- Schuster W. J., Moreno E., Nissen P. E., Pichardo B., 2012, *A&A*, 538, A21
- Schuster W. J., Nissen P. E., 1988, *A&AS*, 73, 225
- Sheffield A. A. et al., 2012, *ApJ*, 761, 161
- Siebert A. et al., 2011, *AJ*, 141, 187
- Smith M. C. et al., 2007, *MNRAS*, 379, 755
- Steinmetz M. et al., 2006, *AJ*, 132, 1645
- Stephens A., Boesgaard A. M., 2002, *AJ*, 123, 1647
- Tillich A., Przybilla N., Scholz R.-D., Heber U., 2009, *A&A*, 507, L37
- Venn K. A., Irwin M., Shetrone M. D., Tout C. A., Hill V., Tolstoy E., 2004, *AJ*, 128, 1177
- Yu Q., Tremaine S., 2003, *ApJ*, 599, 1129
- Zacharias N., Finch C. T., Girard T. M., Henden A., Bartlett J. L., Monet D. G., Zacharias M. I., 2013, *AJ*, 145, 44
- Zhong J. et al., 2014, *ApJLett*, 789, L2
- Zwitter T. et al., 2008, *AJ*, 136, 421